IJMMM International Journal of Minerals, Metallurgy and Materials 矿物冶金与材料学报（英文版）

A gel polymer electrolyte with IL@UiO-66-NH_2 as fillers for high-performance all-solid-state lithium metal batteries

Tao Wei, Qi Zhang, Sijia Wang, Mengting Wang, Ye Liu, Cheng Sun, Yanyan Zhou, Qing Huang, Xiangyun Qiu, and Fang Tian

Cite this article as:
Tao Wei, Qi Zhang, Sijia Wang, Mengting Wang, Ye Liu, Cheng Sun, Yanyan Zhou, Qing Huang, Xiangyun Qiu, and Fang Tian, A gel polymer electrolyte with IL@UiO-66-NH_2 as fillers for high-performance all-solid-state lithium metal batteries, *Int. J. Miner. Metall. Mater.*, 30(2023), No. 10, pp. 1897-1905. https://doi.org/10.1007/s12613-023-2639-0

View the article online at SpringerLink or IJMMM Webpage.

International Journal of Minerals, Metallurgy and Materials
Volume 30, Number 10, October 2023, Page 1897
https://doi.org/10.1007/s12613-023-2639-0

A gel polymer electrolyte with IL@UiO-66-NH_2 as fillers for high-performance all-solid-state lithium metal batteries

Tao Wei[1),✉], *Qi Zhang*[1)], *Sijia Wang*[1)], *Mengting Wang*[1)], *Ye Liu*[1)], *Cheng Sun*[1)], *Yanyan Zhou*[1)], *Qing Huang*[2)], *Xiangyun Qiu*[3)], *and Fang Tian*[4)]

1) School of Energy and Power, Jiangsu University of Science and Technology, Zhenjiang 212003, China
2) College of Materials Science and Engineering, Nanjing Forestry University, Nanjing 210037, China
3) Power & Energy Storage System Research Center, School of Mechanical and Electrical Engineering, Qingdao University, Qingdao 266071, China
4) College of chemical Engineering and Materials, Handan College, Handan 056005, China
(Received: 7 February 2023; revised: 28 March 2023; accepted: 29 March 2023)

Abstract: All solid-state electrolytes have the advantages of good mechanical and thermal properties for safer energy storage, but their energy density has been limited by low ionic conductivity and large interfacial resistance caused by the poor Li^+ transport kinetics due to the solid–solid contacts between the electrodes and the solid-state electrolytes. Herein, a novel gel polymer electrolyte (UPP-5) composed of ionic liquid incorporated metal-organic frameworks nanoparticles (IL@MOFs) is designed, it exhibits satisfying electrochemical performances, consisting of an excellent electrochemical stability window (5.5 V) and an improved Li^+ transference number of 0.52. Moreover, the Li/UPP-5/$LiFePO_4$ full cells present an ultra-stable cycling performance at 0.2C for over 100 cycles almost without any decay in capacities. This study might provide new insight to create an effective Li^+ conductive network for the development of all-solid-state lithium-ion batteries.

Keywords: all solid-state lithium-ion batteries; metal-organic frameworks; gel polymer electrolytes; ionic liquid; solid electrolyte interphase

1. Introduction

In latest decades, the market demand for lithium-ion batteries (LIBs) as an ideal chemical power sources continues to expand with the rapid development of electric or hybrid vehicle fields. However, the traditional LIBs with flammable organic liquid electrolytes have reached its limit of energy density and troubled by the safety issues in practical applications [1–9]. Consequently, the development of next-era higher power density and higher safety rechargeable LIBs is critically urgent [10–15]. Among various candidates that have been reported, all-solid-state lithium-ion batteries (ASSLBs) made up of solid-state electrolytes (SSEs) have caught ever-growing attentions, which is owing to the SSEs possess good electrochemical stability and mechanical/thermal properties. Due to these benefits, SSEs are considered as essential part of ASSLBs. Thus, the performance of ASSLBs can be directly influenced by the characteristics of SSEs [16–21]. However, the existing SSEs also have some shortcomings such as lower ionic conductivity and poorer interface compatibility with solid electrodes compared to liquid electrolytes [22–23].

In recent years, more and more studies have been devoted in exploring new crystalline porous materials as fillers in SSEs. Metal-organic frameworks (MOFs) linked by inorganic metal clusters and organic linkers can be used as the fillers in SSEs for their high specific surface area, large numbers of micropores, and tunable topological geometry [24–26]. In addition, the open metal sites (OMSs) of MOFs can effectively trap anions by Lewis-acid interaction to increase the content of freely moving Li^+ in SSEs [27]. Based on our previous studies [28–29], several SSEs with different kinds of MOFs (UiO-66-NH_2, MIL-100(Fe)) as fillers were prepared, which presented excellent mechanical properties and electrochemical performances. However, the solid–solid contact between the electrodes and the solid-state electrolytes might lead to large interfacial resistances. Fortunately, ionic liquids (ILs) can also be employed as the additives or solvents in SSEs to prepare gel polymer electrolytes (GPEs) for the reason that they have relatively wide electrochemical windows (~6 V) and high ionic conductivity [30–31]. For instance, Xu *et al*. [32] proposed a rational design of different kinds of composite GPEs based on [EMIM][TFSI], rGO-PEG-NH_2, poly(vinylidene) fluoride-hexafluoropropylene (PVDF-HFP), and LiTFSI which showed an ultrahigh electrochemical stability window of 5.0 V and a high ionic conductivity of 2.1×10^{-3} $S \cdot cm^{-1}$ at 30°C, indicating that the electrochemical performances of SSEs can effectively be improved by the IL-based electrolytes. However, the lithium-ion transference number (t_{Li^+}) in IL is inadequate because anions always travel in IL simultaneously with the cations. MOFs with porous

✉ Corresponding author: Tao Wei E-mail: wt863@just.edu.cn, wt863@126.com

structure and plentiful open metal sites (OMSs) have a significant adsorption ability on anions, thus it is a highly feasible technique to load the IL in the pores of MOFs since it could combine the benefits of the IL and MOFs [33]. Subsequently, Wang *et al*. [34] prepared an IL@MOFs composite, i.e., $[EMIM_{0.8}Li_{0.2}][TFSI]$@MOF-525 (Cu), which is benefited from the large pore size of MOF-525 (Cu) (7–12 Å) can allow the IL into it. The results showed that due to the restriction effect of $[TFSI]^-$ by MOFs, an improved t_{Li^+} of 0.36 was obtained, implying the enhancement of electrochemical properties by adding ILs into the pores of MOFs.

In the present work, we designed a novel GPE consisting of activated UiO-66-NH_2, $[PP_{13}][TFSI]$, LiTFSI, and PVDF-HFP by a facile solution-casting method. The Zr-cluster-based MOFs have garnered significant attentions owing to their excellent electrochemical performances and thermal stabilities, thus UiO-66-NH_2 was chosen here. It has a large specific surface area (~809.45 $m^2 \cdot g^{-1}$), which means rich channels and short paths can be provided for the migration of Li^+ [35]. What needs to be pointed out is that the anions ($TFSI^-$) can be trapped by the OMSs of activated UiO-66-NH_2, thus enhances the t_{Li^+} of the GPE, which was reported in our previous study [28]. Moreover, $[PP_{13}][TFSI]$ has a good stability with the Li metal [36–38] which can exhibits excellent electrochemical properties (low viscosity, high conductivity, wide electrochemical window), which is also considered as one of the most promising replacement to the conventional liquid electrolyte. As expected, $[PP_{13}][TFSI]$ is successfully added into the pores of UiO-66-NH_2 (Fig. 1), which shows an improved t_{Li^+} of 0.52, and an ionic conductivity at 60°C of 4.842×10^{-4} $S \cdot cm^{-1}$ with a high electrochemical stability window of 5.5 V. The Li plating/stripping process of the symmetrical cell is almost entirely reversible while cycling and when the GPE was coupled with $LiFePO_4$ (LFP) cathode, the as-prepared ASSLBs can maintain a discharge capacity of 161.9 $mAh \cdot g^{-1}$ at 0.2C after 100 cycles.

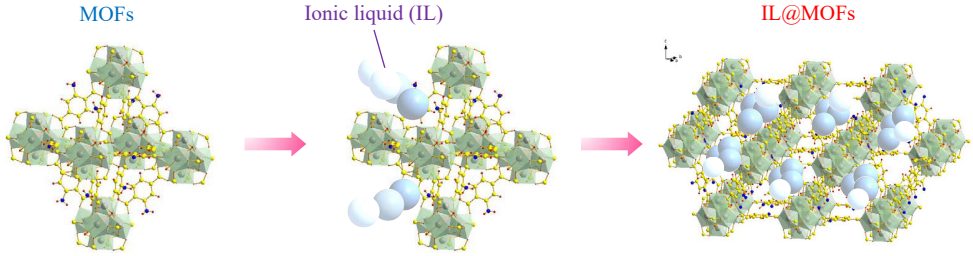

Fig. 1. Schematic diagram of IL incorporated into the pores of MOFs (IL@MOFs).

2. Experimental

2.1. Chemicals

Zirconium (IV) chloride ($ZrCl_4$, 99.9%), 2-aminoterephthalic acid (BDC-NH_2, 98.0%), 1-methyl-2-pyrrolidinone (NMP, 99.0%), N,N-dimethylformamide (DMF, 99.0%), and N,N-dimethylacetamide (DMAc, 99.0%) were purchased from Aladdin; PVDF-HFP (molecular weight ~400000) was acquired from Sigma-Aldrich. Anhydrous ethanol (99.7%) and acetone (99.0%) were purchased from Sinopharm. N-methyl-N-propylpiperidinium bis(trifluoromethanesulfonyl) amide ($[PP_{13}][TFSI]$, 98%) was obtained from Zhengzhou Alfa Chemical Co., Ltd., China

2.2. Synthesis of UiO-66-NH_2

The MOF UiO-66-NH_2 was synthesized by a facile solvothermal method as our previous study. Firstly, BDC-NH_2 (0.186 g) and $ZrCl_4$ (0.240 g) were dissolved in N,N-thdimethylformamide (DMF, 60 mL), and magnetically stirred for 45 min at 25°C to acquire a homogeneous mixture. Then, the homogeneous mixture was transferred into a 100 mL Teflon liner via heating at 120°C for 24 h. Finally, the yellow suspension was collected by centrifugation and washed repeatedly with the mixed solution of DMF and ethanol, the collected product was dried at 80°C under vacuum overnight, the yellow UiO-66-NH_2 powers were obtained in the end. The powder was activated overnight at 150°C under vacuum before each application.

2.3. Incorporation of $[PP_{13}][TFSI]$ in UiO-66-NH_2

The prepared UiO-66-NH_2 have been incorporated separately with 30wt%, 40wt%, and 50wt% of N-methyl-N-propylpiperidinium bis(trifluoromethanesulfonyl)imide ($[PP_{13}][TFSI]$) using mortar and pestle. And then the $[PP_{13}][TFSI]$ has been incorporated into the micropores of UiO-66-NH_2, which named as IL@MOFs ($[PP_{13}][TFSI]$@UiO-66-NH_2). The obtained nanocomposites have been heated at 150°C for 12 h to dry off the water content of materials, which is also beneficial for homogeneous distribution of IL inside the pores of MOFs.

2.4. Preparation of GPEs membranes

The GPEs membranes were prepared by a facile coating technique. Firstly, a certain mass of PVDF-HFP and LiTFSI were dissolved in a mixture solution of N,N-dimethylacetamide (DMAc) and acetone (volume ratio, $v : v$ is 1:2). Following that, the solution was magnetically stirred at 70°C for 3 h until no large particles were presented. And then, a certain amount of IL@MOFs was added to the slurry and stirred overnight at 50°C. Next, coating the slurry evenly on the PTFE plate with a scraper and following which is drying it at 60°C for 24 h. Finally, the dried GPEs membranes were punched into ϕ18 mm disks and put it in the glove box for further use.

3. Results and discussion

3.1. Material characterization

Fig. 2(a) presented the schematic illustration of fabrication process of IL@MOFs via a facile mixed grinding method (details can be seen in the supplementary information). Fig. 2(b) revealed a phenomenon that with the increase of the amount of IL, the color of the powder changes from light to dark, which means IL has been absorbed into the pores of MOFs. In addition, MOFs after adding 30wt%, 40wt%, and 50wt% of IL is powdery, but when the adding-proportion is more than 50wt%, the powder becomes argillaceous, which might be caused by too much of IL (Fig. 2(b)). It should be noted that the addition of excessive IL (>50wt%) will make the IL@MOFs nanoparticles into a sticky state, which introduces more uncertainty in the experimental operation, so more IL in MOFs is not considered in this work. The X-ray diffraction (XRD) patterns of four kinds of IL@MOFs powders are depicted in Fig. 2(c). The remarkable crystallinity of UiO-66-NH_2 is demonstrated by the two prominent characteristic peaks at roughly 7.4° and 8.5°, which correspond to the (111) and (002) planes, respectively. From the scanning electron microscope (SEM) images in Fig. S1, nicely ordered distribution of UiO-66-NH_2 nanoparticles with 50wt% IL can be observed, and there are also some granular agglomerated particles presented, which might form mesopores in the nanocomposite system [39]. In order to further prove that [PP_{13}][TFSI] were successfully added into the pores of UiO-66-NH_2, nitrogen (N_2) adsorption/desorption tests were conducted, which were presented in Fig. 2(d)–(f). It can be concluded that as the weight percentage of IL increases, N_2 adsorption at low relative pressure falls because the IL preferentially entrap in the MOFs' micropores rather than their mesopores [40], which significantly decreases the total surface area of UiO-66-NH_2 (Fig. S2). The N_2 adsorption/desorption isotherms are significantly influenced when IL is confined in the micropores of MOFs. Furthermore, the total surface area also decreases with the increased concentration of IL in the nanocomposites along with N_2 absorbed sites, which are given in Table S1. According to the above results, it can be preliminarily concluded that the IL is successfully loaded into the pores of MOFs.

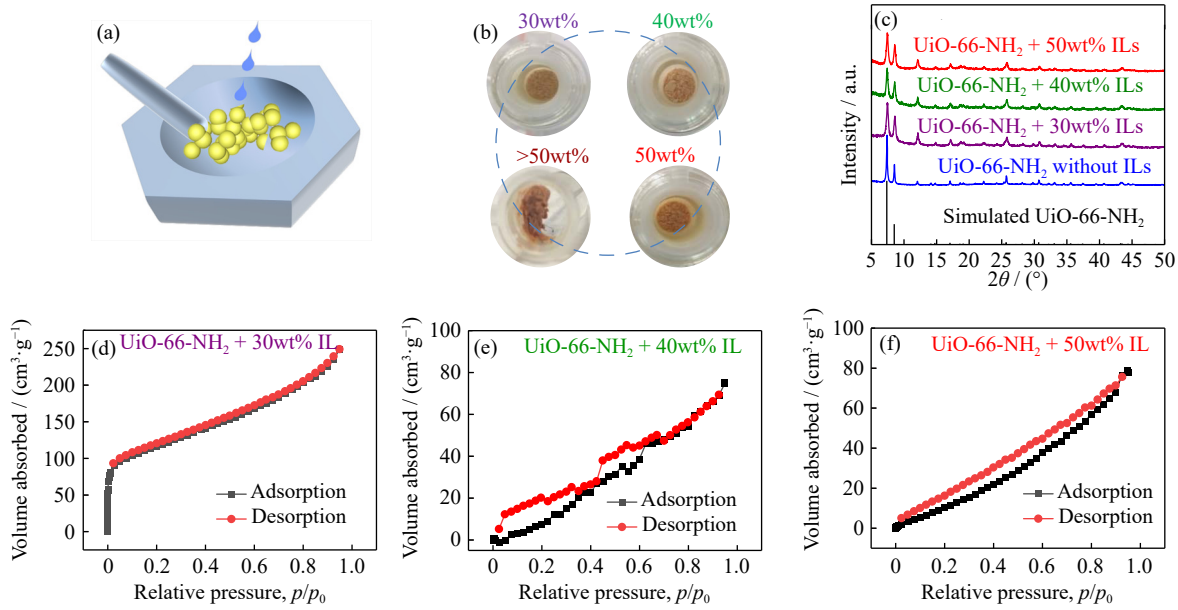

Fig. 2. (a) Schematic diagram of the preparation process of IL@MOFs. (b) Digital photos of IL@MOFs (with 30wt%, 40wt%, 50wt%, and >50wt% IL of IL@MOFs). (c) XRD patterns of four kinds of IL@MOFs powders. (d–f) N_2 absorption/desorption isotherms of IL@MOFs (with IL of 30wt% (d), 40wt% (e), and 50wt% (f)).

The above four kinds of IL@MOFs nanocomposites were gradually added into the PVDF-HFP matrix to prepare various GPEs (according to the amount of IL, denoted as UPP-0, UPP-3, UPP-4, and UPP-5, respectively) (Fig. 3(a)), which are all smooth and flat. To better observe the microscopic morphology of these as-prepared GPEs, the representative SEM images of UPP-5 are presented in Fig. 3(b) and (c). Fig. 3(b) shows the surface SEM image of UPP-5, which is clearly that some irregular blocks and gaps are present. On one hand, the irregular blocks are attributed to the fact that polymer matrix swells and encloses LiTFSI, [PP_{13}][TFSI], and UiO-66-NH_2. On the other hand, the gaps are may be ascribed to the loose arrangement of PVDF-HFP matrix. While in the cross-sectional image (Fig. 3(c)), the membrane is continuous, free of visible pore structures but with some wrinkles, which in accordance with Fig. 3(b). In addition, it can also be clearly seen that the thickness of the membrane is about 75 μm. What's more, the uniform distribution of the elements F, S, Zr, and N in Fig. 3(d)–(g) further demonstrated that the 50wt% [PP_{13}][TFSI]@UiO-66-NH_2 nanoparticles are dispersed evenly throughout the PVDF-HFP matrix and without noticeable agglomeration.

3.2. Electrochemical performance

The GPEs were sandwiched between two steel electrodes, and electrochemical impedance spectroscopy (EIS) tests

were performed to test the ionic conductivity of different GPEs. From the results described in Fig. 4(a) and Fig. S3, the impedance of the UPP-5 is minimal at all temperatures, which is owing to the IL being fixed in the pores of MOFs,

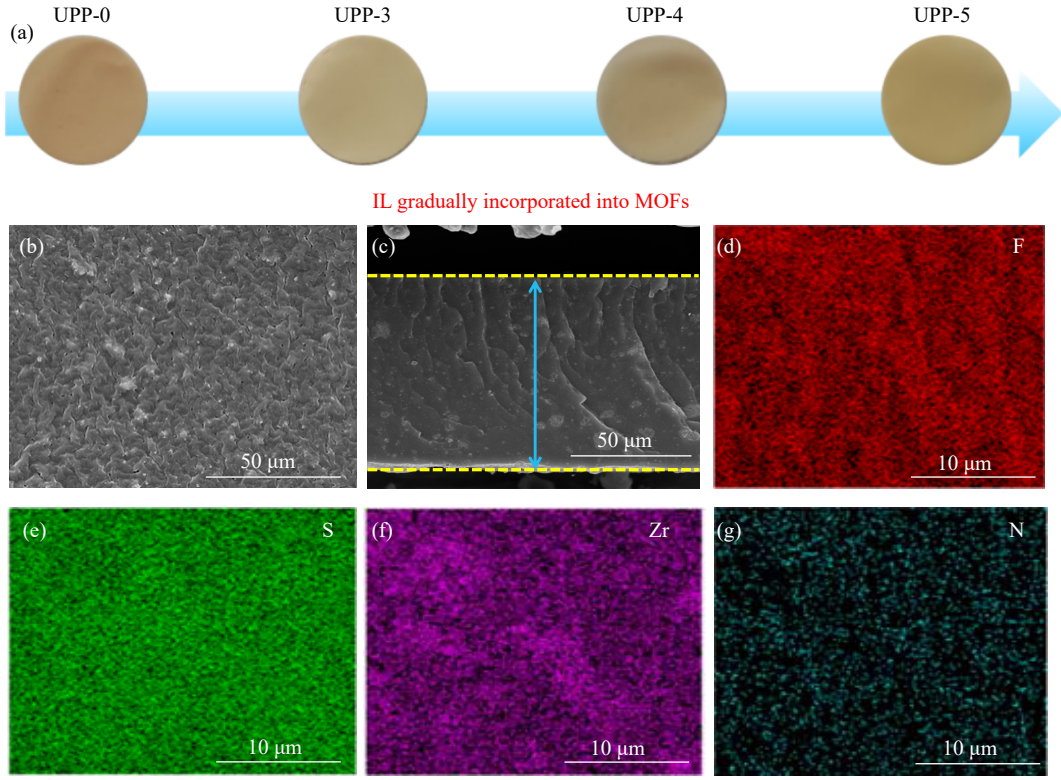

Fig. 3. (a) Digital photos of various GPEs (UPP-0, UPP-3, UPP-4, and UPP-5); (b, c) SEM images of UPP-5 GPEs: (b) surface; (c) cross-sectional; (d–g) EDS mapping images of different elements in UPP-5 GPEs: (d) F, (e) S, (f) Zr, and (g) N.

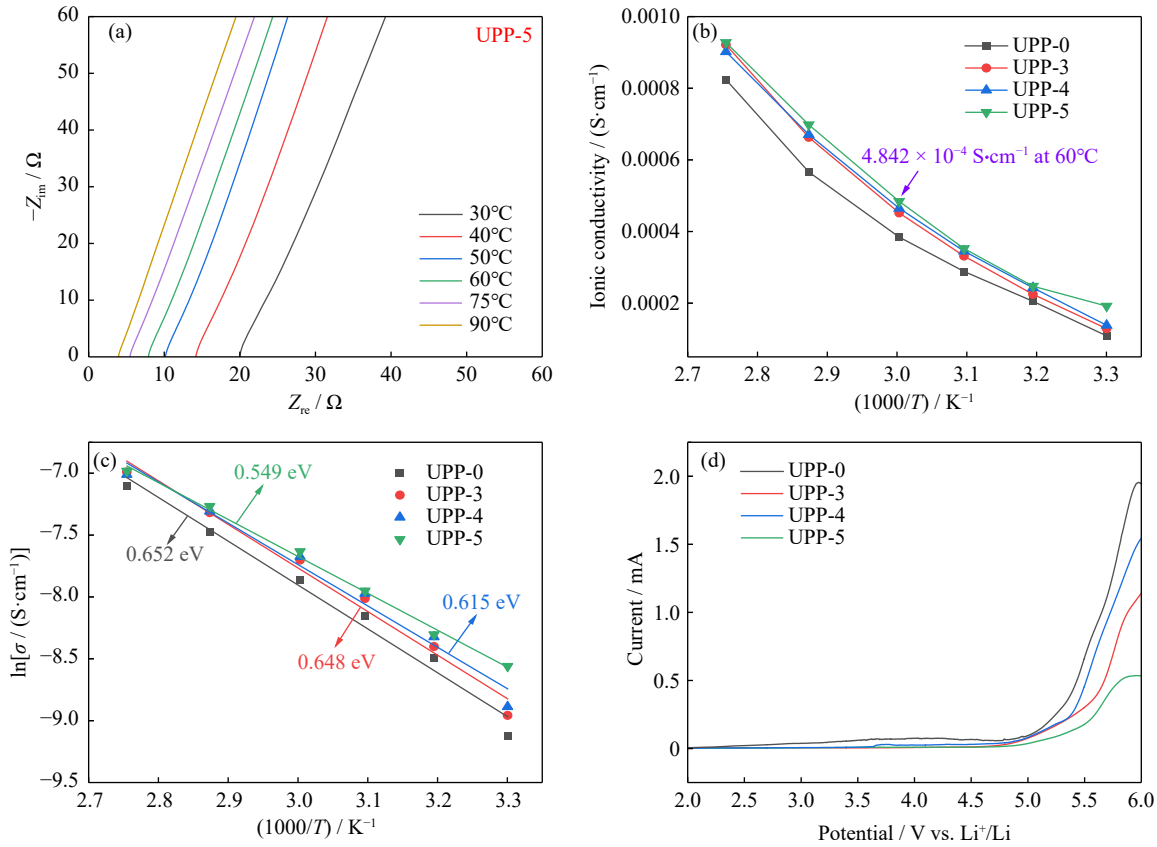

Fig. 4. (a) Temperature-dependent EIS spectroscopy curves for UPP-5 GPE; (b) ionic conductivities of different GPEs; (c) Arrhenius plots of various GPEs at different temperatures; (d) the curves of LSV for different GPEs at a scan rate of 1 mV·s^{-1}.

thus the proper addition of IL plays a positive role on the promotion of Li^+ transport. Compared with the other GPEs (UPP-0, UPP-3, and UPP-4), UPP-5 has the highest ionic conductivity at 60°C (4.842×10^{-4} S·cm^{-1}, Fig. 4(b)). It can be clearly seen that the ionic conductivities of another two GPEs with IL@MOFs (UPP-3, UPP-4) were relatively lower (4.52×10^{-4} and 4.64×10^{-4} S·cm^{-1}, respectively). Such a high ionic conductivity of UPP-5 might be resulted in the reasons as follows. Firstly, uniformly distribution of UiO-66-NH_2 (Zr) significantly decreases the crystalline phase of PVDF-HFP in the polymer matrix, which further suppresses the fractional reconfiguration of the polymer chains and this leads to more amorphous phases in the polymer matrix and thus promote the transfer of lithium-ion, because the mobility of Li^+ relies on the amorphous phases in the PVDF-HFP polymer [28]. Secondly, there are many sub-nanopores in UiO-66-NH_2, which could provide fast channels for Li^+ migration; Thirdly, the addition of [PP_{13}][TFSI] can weaken the correlation between $TFSI^-$ of lithium salt and Li^+ by binding anions effectively and produce more free Li^+, which further promotes the migration of lithium-ions [41–42]. What's more, the contact between the electrodes and the GPE could also be improved by the IL. Fig. 4(c) presents the Arrhenius plots of the GPEs and according to the linear fitting results, the ionic conductivity complies with the Arrhenius equation [43]. According to the slope of the fitting line in Fig. 4(c) and Eq. (1), the activation energy (E_a) can be obtained.

$$\sigma = \sigma_0 \exp(-\frac{E_a}{RT}) \quad (1)$$

where R represents the molar gas constant (8.314 J·K^{-1}·mol^{-1}) and the σ_0 is the pre-exponential factor.

It can be found that the E_a of UPP-0 (0.652 eV), UPP-3 (0.648 eV), and UPP-4 (0.615 eV) are all higher than that of UPP-5 (0.549 eV). It was concluded in our previous study that the bigger the value of E_a, the higher the lithium-ion migration barrier is [44], which implies adding [PP_{13}][TFSI]@UiO-66-NH_2 nanoparticles into GPEs is a conducive way to provide a fast channel for Li^+ transportation.

The electrochemical stability windows of GPEs were tested at room temperature by linear sweep voltammetry (LSV) (Fig. 4(d)). The pure PVDF-HFP electrolytes without the additives are decomposed at about 4.2 V according to a previous study [45], while the GPEs with 30wt% and 40wt% IL@MOFs (UPP-3 and UPP-4) are decomposed at ~5.0 V vs. Li/Li^+. More importantly, the electrochemical stability window of UPP-5 is up to ~5.5 V, which could be owing to the facts that the structural stability of GPEs at high voltage is strengthened by the Lewis acid-base interaction and the hydrogen bonds between –NH_2 groups of MOFs and F atoms on PVDF-HFP chains [28], and meanwhile the [PP_{13}][TFSI] with a wider electrochemical window has positive effects as well. The results show that adding [PP_{13}][TFSI] into the nanopores of UiO-66-NH_2 can effectively improve the electrochemical stability of GPEs.

Based on the above results, UPP-5 has the best performances, so UPP-5 was chosen for further characterizations. The t_{Li^+} of UPP-5 was evaluated through a potentiostatic polarization way, symmetric cells with UPP-5 sandwiched between two Li foils were characterized by using the direct current (DC) polarization and EIS measurements. The result is shown in Table S2. It is noteworthy that UPP-5 has a relatively higher t_{Li^+} of 0.52 than that of traditional liquid electrolyte (~0.40) [46], which is simultaneously superior than other IL-based electrolytes in previous studies [47–48]. This might be due to that on one hand, lithium salt (LiTFSI) can be dissociated and dissolved more quickly by cooperating the lone pair electrons in high density electron-donating groups for the high dielectric constant of PVDF-HFP. On the other hand, the anions of $TFSI^-$ are confined and bonded by the open metal sites (OMSs) of the MOFs, which allows lithium-ions to a more easily pass through the channel.

For further determine the stability of lithium anodes and IL@MOFs-based GPE, the electrochemical stability of UPP-5 coupled with Li metal using symmetric Li/UPP-5/Li cells was tested at 0.05 mA·cm^{-2}, which was presented in Fig. 5(a). It can be demonstrated that the UPP-5 has a gentle Li plating and stripping plateaus with a minor nucleation overpotential as tiny as 50–60 mV during cycling, and can perform highly stable for up to 1000 h without experiencing an internal short circuit, which indicates the UPP-5 GPE has remarkable stability against lithium metal and it can achieve reversible lithium deposition, which could be due to the following factors: (1) the appropriate amount of [PP_{13}][TFSI] added into the pores of UiO-66-NH_2 can promote an uniform deposition of lithium-ions effectively; (2) the IL [PP_{13}][TFSI] has a superior stability against Li metal [38]. What's more, the cell was run for 2 h per cycle under various current densities from 0.05 to 0.4 mA·cm^{-2} at 60°C (Fig. 5(b)), which maintains a small polarization voltage 7.6, 16.9, 33.9, and 72.6 mV, respectively. As the current density rises, all of the voltage plateaus remain steady without experiencing too many notable changes. Undoubtedly, UPP-5 has an excellent interfacial stability with metallic lithium, which was demonstrated by an EIS test before and after cycling in symmetric Li cells (Fig. S4). It can be clearly found that the interface resistance has become lower after 30 cycles (~72.52 Ω) than that before cycling (~82.24 Ω), which might be for the reason that a stable solid electrolyte interphase (SEI) layer was formed [38]. In addition, Fig. S5 compares the EIS results in symmetric Li cells with two kinds of GPEs before and after 100 cycles (UPP-0 and UPP-5), which further illustrates the stable SEI was formed as a result of the appropriate addition of IL. These results might be attributed to that [PP_{13}][TFSI] can improve the lithium-ion diffusion capacity and act as a bridge for the transfer of Li^+ at the electrolyte/electrode interface [49].

To further study the cycling stability of GPEs in ASSLBs, two different SSEs (UPP-0, UPP-5) were regarded as separators, sandwiched with LFP cathode and Li foil anode, and the obtained CR2032 coin cells were firstly tested for the galvanostatic charge–discharge cycles at 60°C (Fig. 6(a) and (b)). It can be clearly found that in Fig. 6(a), the ASSLBs assembled with UPP-0 failed to keep a stable Coulombic effi-

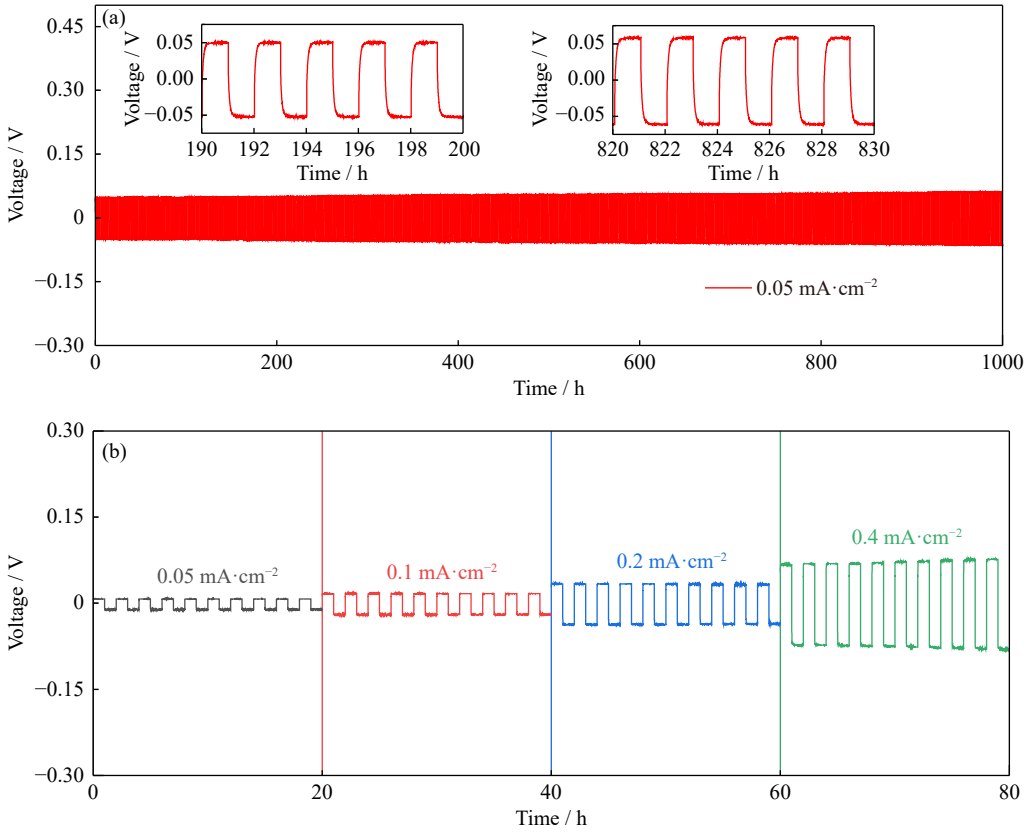

Fig. 5. (a) Galvanostatic cycling curve of Li/UPP-5/Li cells at 0.05 mA·cm^{-2} at 60°C; (b) rate performances of Li/UPP-5/Li cells at various current densities at 60°C.

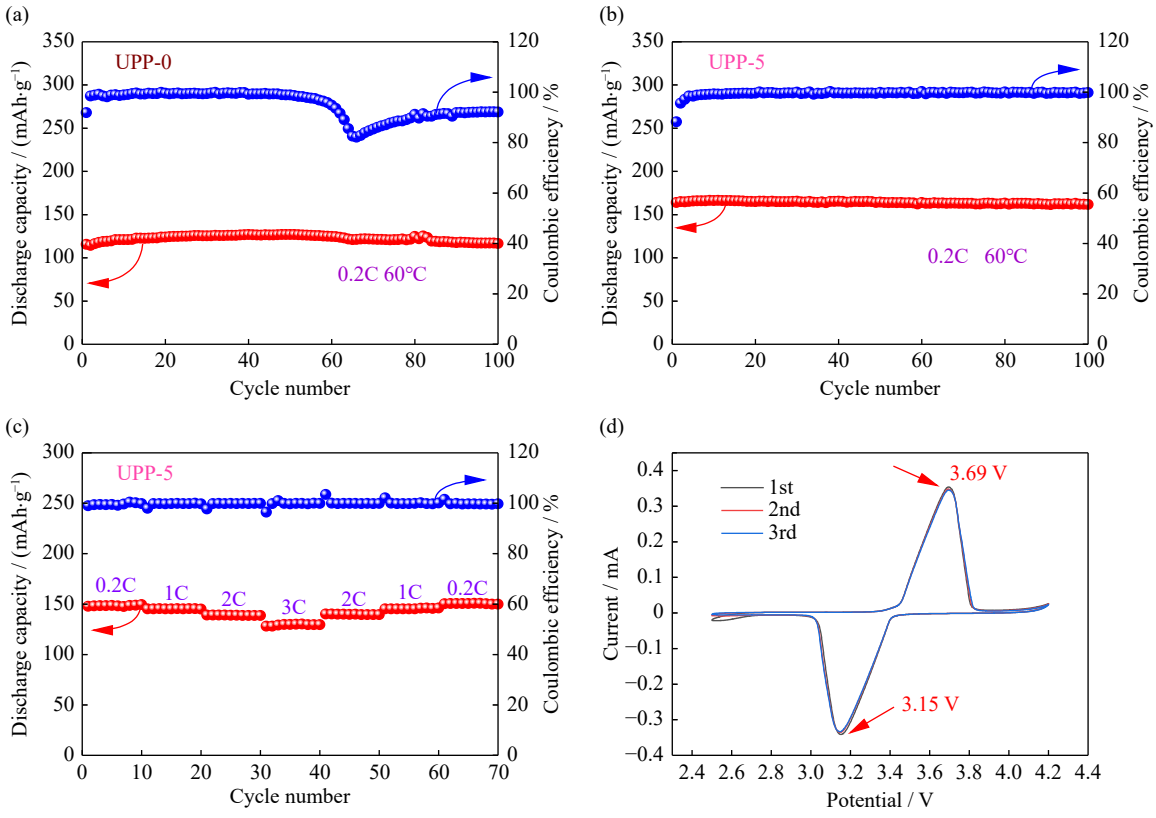

Fig. 6. Cycling performances in full batteries for various GPEs at 0.2C of (a) UPP-0 and (b) UPP-5; (c) rate properties of the cell with UPP-5 between 0.2C and 3C (0.2C, 1C, 2C, and 3C); (d) CV curves of the initial Li/UPP-5/LFP cells at 0.1 mV·s^{-1}. All the tests were operated at 60°C.

ciency in 100 cycles, which might be attributed to the poor interface compatibility between the electrodes and the UPP-0. By comparison, the ASSLBs with UPP-5 can cycle for over 100 cycles at 0.2C (1C = 170 mAh·g^{-1}) without any decrease (Fig. 6(b)), which might be ascribed to a stable SEI can be formed by adding moderate [PP_{13}][TFSI] into gel polymer electrolytes (GPEs) [50]. In addition, the stable SEI film is an electronic insulation and Li^+ conductive film, which is also the reason why lithium-ions can be transmitted rapidly at the electrolyte/electrode interfaces [36]. Fig. 6(c) depicted the rate properties of the Li/UPP-5/LFP full cell between 0.2C and 3C. The first discharge capacities are 147.8, 145.2, 139.0, and 128.0 mAh·g^{-1} at 0.2C, 1C, 2C, and 3C, respectively. After backing to 0.2C, the capacity is without any decrease and maintained at 150.3 mAh·g^{-1}, which suggests that the full cell assembled with UPP-5 has a superior electrochemical reversibility. In addition, the cyclic voltammetry (CV) tests of the Li/UPP-5/LFP full cells were also conducted and presented in Fig. 6(d). From Fig. 6(d), the reduction and oxidation potentials (3.15 V and 3.69 V) in the first three cycles overlapped very well, which means that the formed SEI film can be stabilized during the charging/discharging processes and this is consistent with our previous studies in the fields of solid polymer-based electrolytes [28–29,44].

3.3. Mechanisms

In a word, the GPEs with [PP_{13}][TFSI]@UiO-66-NH_2, which possibly can effectively promote the growth of a stable SEI layer and further improve the interface stability between electrode and electrolyte of ASSLBs, which could be demonstrated from the SEM images of Li electrodes after cycling in Li/UPP-0/LFP and Li/UPP-5/LFP full cells (Fig. 7) [51–52]. Meanwhile, the anions ($TFSI^-$) can be trapped rapidly by the OMSs of activated UiO-66-NH_2, thus enhances the t_{Li^+} of the GPE through Lewis acid-base interaction and the hydrogen bonds between –NH_2 groups of UiO-66-NH_2 and F atoms of PVDF-HFP chains can improve the structural stability of the GPE. More importantly, the addition of ILs will significantly increase the free Li^+ in the electrolyte by fixing anions (Fig. 8). Based on the above discussions, the excellent electrochemical performance of Li/UPP-5/LFP battery makes the novel UPP-5 GPE highly promising for future solid-state LIBs.

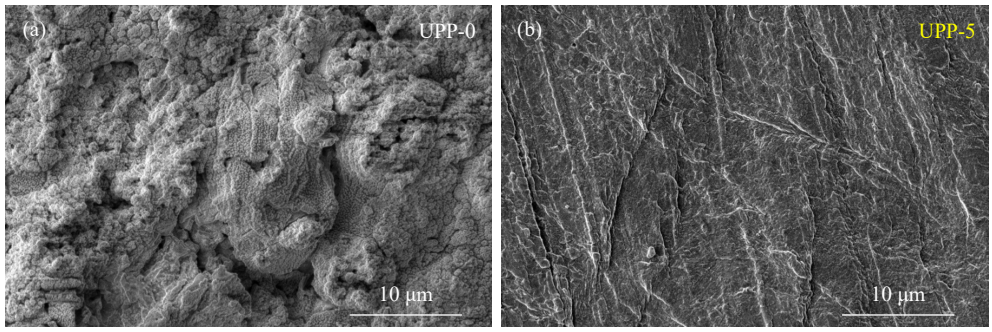

Fig. 7. SEM images of Li electrodes after cycling in different full cells: (a) Li/UPP-0/LFP; (b) Li/UPP-5/LFP.

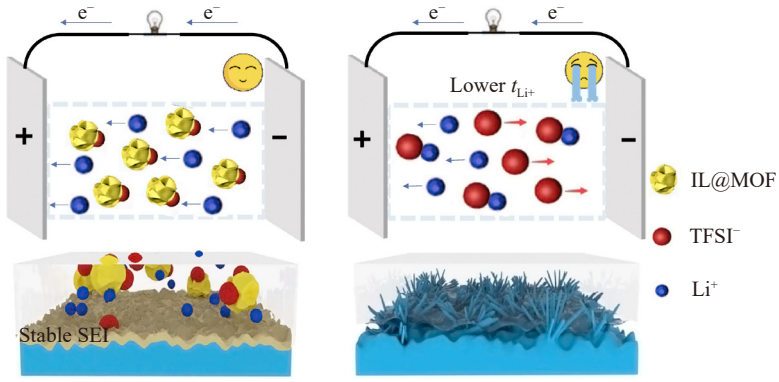

Fig. 8. Possible mechanisms of the formation of a more stable SEI layer through GPEs and the synergistic effect of IL and MOFs.

4. Conclusion

To sum up, this work successfully introduced an IL ([PP_{13}][TFSI]) into the MOFs (UiO-66-NH_2) to prepare a novel GPE UPP-5, which provides a stable electrolyte/electrode interface for Li electrodeposition. The UPP-5 GPE possesses an improved Li^+ transference number of 0.52, and good compatibilities with Li metal with a high electrochemical stability window of about 5.5 V. Evidently, the UPP-5 can guide uniform Li deposition by forming a protective SEI film on Li metal, which effectively suppress the growth of Li dendrite. Furthermore, Li/LFP full cell with the electrolyte of UPP-5 exhibits a capacity of ~160 mAh·g^{-1} at 0.2C for more than 100 cycles without any decay. We believe that the

IL@MOFs-based GPE (UPP-5) is a promising strategy for addressing problems of Li dendritic growth and promote a further development of ASSLBs.

Acknowledgement

This work was financially supported by National Natural Science Foundation of China (No. 21701083).

Conflict of Interest

The authors declare no competing financial interest.

Supplementary Information

The online version contains supplementary material available at https://doi.org/10.1007/s12613-023-2639-0.

References

[1] M.S. Balogun, W.T. Qiu, Y. Luo, *et al*., A review of the development of full cell lithium-ion batteries: The impact of nanostructured anode materials, *Nano Res.*, 9(2016), No. 10, p. 2823.

[2] J. Liu, Z.N. Bao, Y. Cui, *et al*., Pathways for practical high-energy long-cycling lithium metal batteries, *Nat. Energy*, 4(2019), No. 3, p. 180.

[3] Y. Wang, W.D. Richards, S.P. Ong, *et al*., Design principles for solid-state lithium superionic conductors, *Nat. Mater.*, 14(2015), No. 10, p. 1026.

[4] C. Yu, S. Ganapathy, E.R.H. van Eck, *et al*., Accessing the bottleneck in all-solid state batteries, lithium-ion transport over the solid-electrolyte-electrode interface, *Nat. Commun.*, 8(2017), No. 1, art. No. 1086.

[5] Y.L. Zhao, X.Z. Yuan, L.B. Jiang, *et al*., Regeneration and reutilization of cathode materials from spent lithium-ion batteries, *Chem. Eng. J.*, 383(2020), art. No. 123089.

[6] T. Wei, Z.H. Zhang, Z.Y. Zhu, *et al*., Recycling of waste plastics and scalable preparation of Si/CNF/C composite as anode material for lithium-ion batteries, *Ionics*, 25(2019), No. 4, p. 1523.

[7] J.B. Zhou, P. Chen, W. Wang, and X. Zhang, $Li_7P_3S_{11}$ electrolyte for all-solid-state lithium-ion batteries: Structure, synthesis, and applications, *Chem. Eng. J.*, 446(2022), art. No. 137041.

[8] F.Y. Wang, Y.S. Ye, Z.M. Wang, *et al*., MOF-derived Co_3O_4@rGO nanocomposites as anodes for high-performance lithium-ion batteries, *Ionics*, 27(2021), No. 10, p. 4197.

[9] T. Wei, Y.Y. Zhou, C. Sun, *et al*., Prestoring lithium into SnO_2 coated 3D carbon fiber cloth framework as dendrite-free lithium metal anode, *Particuology*, 84(2024), p. 89.

[10] Z.H. Chen, I. Belharouak, Y.K. Sun, and K. Amine, Titanium-based anode materials for safe lithium-ion batteries, *Adv. Funct. Mater.*, 23(2013), No. 8, p. 959.

[11] Z.H. Gao, S. Rao, T.Y. Zhang, *et al*., Design strategies of flame-retardant additives for lithium ion electrolyte, *J. Electrochem. Energy Convers. Storage*, 19(2022), No. 3, art. No. 030910.

[12] L.P. Zhang, X.L. Li, M.R. Yang, and W.H. Chen, High-safety separators for lithium-ion batteries and sodium-ion batteries: Advances and perspective, *Energy Storage Mater.*, 41(2021), p. 522.

[13] Z.H. Zhang, T. Wei, J.H. Lu, *et al*., Practical development and challenges of garnet-structured $Li_7La_3Zr_2O_{12}$ electrolytes for all-solid-state lithium-ion batteries: A review, *Int. J. Miner. Metall. Mater.*, 28(2021), No. 10, p. 1565.

[14] D. Zhou, D. Shanmukaraj, A. Tkacheva, M. Armand, and G.X. Wang, Polymer electrolytes for lithium-based batteries: Advances and prospects, *Chem*, 5(2019), No. 9, p. 2326.

[15] J.H. Lu, Z.M. Wang, Q. Zhang, *et al*., The effects of amino groups and open metal sites of MOFs on polymer-based electrolytes for all-solid-state lithium metal batteries, *Chin. J. Chem. Eng.*, (2023)

[16] Z.F. Ruan, Y.Z. Du, H.F. Pan, *et al*., Incorporation of poly(ionic liquid) with PVDF-HFP-based polymer electrolyte for all-solid-state lithium-ion batteries, *Polymers*, 14(2022), No. 10, art. No. 1950.

[17] X.X. Wu, K.Y. Chen, Z.G. Yao, *et al*., Metal organic framework reinforced polymer electrolyte with high cation transference number to enable dendrite-free solid state Li metal conversion batteries, *J. Power Sources*, 501(2021), art. No. 229946.

[18] Z.L. Xiao, T.Y. Long, L.B. Song, Y.H. Zheng, and C. Wang, Research progress of polymer-inorganic filler solid composite electrolyte for lithium-ion batteries, *Ionics*, 28(2022), No. 1, p. 15.

[19] Q.Y. Guo, F.L. Xu, L. Shen, *et al*., 20 μ m-thick $Li_{6.4}La_3Zr_{1.4}Ta_{0.6}O_{12}$-based flexible solid electrolytes for all-solid-state lithium batteries, *Energy Mater. Adv.*, 2022(2022), art. No. 9753506.

[20] Z.Y. Wang, L. Shen, S.G. Deng, P. Cui, and X.Y. Yao, 10 μm-thick high-strength solid polymer electrolytes with excellent interface compatibility for flexible all-solid-state lithium-metal batteries, *Adv. Mater.*, 33(2021), No. 25, art. No. 2100353.

[21] Q. Zhang, S.J. Wang, Y. Liu, *et al*., UiO-66-NH_2 @67 core–shell metal-organic framework as fillers in solid composite electrolytes for high-performance all-solid-state lithium metal batteries, *Energy Technol.*, 11(2023), No. 4, art. No. 2201438.

[22] C.W. Sun, J. Liu, Y.D. Gong, D.P. Wilkinson, and J.J. Zhang, Recent advances in all-solid-state rechargeable lithium batteries, *Nano Energy*, 33(2017), p. 363.

[23] Q.Q. Zhang, K. Liu, F. Ding, and X.J. Liu, Recent advances in solid polymer electrolytes for lithium batteries, *Nano Res.*, 10(2017), No. 12, p. 4139.

[24] R. Dutta and A. Kumar, Ion transport dynamics in ionic liquid incorporated CuBTC-metal-organic framework based composite polymer electrolyte, *J. Mater. Sci.*, 30(2019), No. 2, p. 1117.

[25] T. Wei, J.H. Lu, P. Zhang, *et al*., Metal-organic framework-derived Co_3O_4 modified nickel foam-based dendrite-free anode for robust lithium metal batteries, *Chin. Chem. Lett.*, (2022), art. No. 107947.

[26] T. Wei, J.H. Lu, M.T. Wang, *et al*., MOF-derived materials enabled lithiophilic 3D hosts for lithium metal anode—A review, *Chin. J. Chem.*, 2023. DOI: 10.1002/cjoc.202200816

[27] Q.Y. Han, S.Q. Wang, Z.Y. Jiang, X.C. Hu, and H.H. Wang, Composite polymer electrolyte incorporating metal-organic framework nanosheets with improved electrochemical stability for all-solid-state Li metal batteries, *ACS Appl. Mater. Interfaces*, 12(2020), No. 18, p. 20514.

[28] T. Wei, Z.H. Zhang, Q. Zhang, *et al*., Anion-immobilized solid composite electrolytes based on metal-organic frameworks and superacid ZrO_2 fillers for high-performance all solid-state lithium metal batteries, *Int. J. Miner. Metall. Mater.*, 28(2021), No. 10, p. 1636.

[29] T. Wei, Z.M. Wang, M. Zhang, *et al*., Activated metal-organic frameworks (a-MIL-100 (Fe)) as fillers in polymer electrolyte for high-performance all-solid-state lithium metal batteries, *Mater. Today Commun.*, 31(2022), art. No. 103518.

[30] Z.E. Liu, Z.W. Hu, X.A. Jiang, *et al*., Metal-organic framework confined solvent ionic liquid enables long cycling life quasi-solid-state lithium battery in wide temperature range, *Small*,

18(2022), No. 37, art. No. 2203011.
[31] X. Tang, S.Y. Lv, K. Jiang, G.H. Zhou, and X.M. Liu, Recent development of ionic liquid-based electrolytes in lithium-ion batteries, *J. Power Sources*, 542(2022), art. No. 231792.
[32] P. Xu, H.Y. Chen, X. Zhou, and H.F. Xiang, Gel polymer electrolyte based on PVDF-HFP matrix composited with rGO-PEG-NH_2 for high-performance lithium ion battery, *J. Membr. Sci.*, 617(2021), art. No. 118660.
[33] T. Wei, Z.M. Wang, Q. Zhang, *et al*., Metal-organic framework-based solid-state electrolytes for all solid-state lithium metal batteries: A review, *CrystEngComm*, 24(2022), No. 28, p. 5014.
[34] Z.Q. Wang, R. Tan, H.B. Wang, *et al*., A metal-organic-framework-based electrolyte with nanowetted interfaces for high-energy-density solid-state lithium battery, *Adv. Mater.*, 30(2018), No. 2, art. No. 1704436.
[35] Y. Liu, Q.H. Zeng, P.P. Chen, *et al*., Modified MOF-based composite all-solid-state polymer electrolyte with improved comprehensive performance for dendrite-free Li-ion batteries, *Macromol. Chem. Phys.*, 223(2022), No. 8, art. No. 2100325.
[36] J. Reiter and M. Nadherna, *N*-Allyl-*N*-methylpiperidinium bis(trifluoromethanesulfonyl)imide—A film forming ionic liquid for graphite anode of Li-ion batteries, *Electrochim. Acta*, 71(2012), p. 22.
[37] X.M. Gao, Q.T. Qu, G.B. Zhu, *et al*., Piperidinium-based ionic liquid electrolyte with linear solvent and LiODFB for $LiFePO_4$/Li cells at room and high temperature, *RSC Adv.*, 7(2017), No. 79, p. 50135.
[38] C.B. Zhu, H. Cheng, and Y. Yang, Electrochemical characterization of two types of PEO-based polymer electrolytes with room-temperature ionic liquids, *J. Electrochem. Soc.*, 155(2008), No. 8, art. No. A569.
[39] R. Dutta and A. Kumar, Dielectric relaxation dynamics and AC conductivity scaling of metal-organic framework (MOF-5) based polymer electrolyte nanocomposites incorporated with ionic liquid, *J. Phys. D: Appl. Phys.*, 50(2017), No. 42, art. No. 425302.
[40] K. Fujie, K. Otsubo, R. Ikeda, T. Yamada, and H. Kitagawa, Low temperature ionic conductor: Ionic liquid incorporated within a metal-organic framework, *Chem. Sci.*, 6(2015), No. 7, p. 4306.
[41] Z.L. Hu, X.J. Zhang, and S.M. Chen, A graphene oxide and ionic liquid assisted anion-immobilized polymer electrolyte with high ionic conductivity for dendrite-free lithium metal batteries, *J. Power Sources*, 477(2020), art. No. 228754.
[42] T.H. Zhou, Y. Zhao, J.W. Choi, and A. Coskun, Ionic liquid functionalized gel polymer electrolytes for stable lithium metal batteries, *Angew. Chem. Int. Ed.*, 60(2021), No. 42, p. 22791.
[43] T. Wei, Z.H. Zhang, Z.M. Wang, *et al*., Ultrathin solid composite electrolyte based on $Li_{6.4}La_3Zr_{1.4}Ta_{0.6}O_{12}$/PVDF-HFP/LiTFSI/succinonitrile for high-performance solid-state lithium metal batteries, *ACS Appl. Energy Mater.*, 3(2020), No. 9, p. 9428.
[44] Q. Zhang, T. Wei, J.H. Lu, *et al*., The effects of PVB additives in MOFs-based solid composite electrolytes for all-solid-state lithium metal batteries, *J. Electroanal. Chem.*, 926(2022), art. No. 116935.
[45] N. Chen, Y. Xing, L.L. Wang, *et al*., "Tai Chi" philosophy driven rigid-flexible hybrid ionogel electrolyte for high-performance lithium battery, *Nano Energy*, 47(2018), p. 35.
[46] Q.H. Zeng, J.A. Wang, X. Li, *et al*., Cross-linked chains of metal-organic framework afford continuous ion transport in solid batteries, *ACS Energy Lett.*, 6(2021), No. 7, p. 2434.
[47] J.F. Wu and X. Guo, Nanostructured metal-organic framework (MOF)-derived solid electrolytes realizing fast lithium ion transportation kinetics in solid-state batteries, *Small*, 15(2019), No. 27, art. No. 1902429.
[48] K. Wang, L.Y. Yang, Z.Q. Wang, *et al*., Enhanced lithium dendrite suppressing capability enabled by a solid-like electrolyte with different-sized nanoparticles, *Chem. Commun.*, 54(2018), No. 93, p. 13060.
[49] M. Liu, S. Zhang, E.R.H. van Eck, C. Wang, S. Ganapathy, and M. Wagemaker, Improving Li-ion interfacial transport in hybrid solid electrolytes, *Nat. Nanotechnol.*, 17(2022), No. 9, p. 959.
[50] Z.J. Bi, N. Zhao, L.N. Ma, *et al*., Interface engineering on cathode side for solid garnet batteries, *Chem. Eng. J.*, 387(2020), art. No. 124089.
[51] K.X. Liu, Z.Y. Wang, L.Y. Shi, S. Jungsuttiwong, and S. Yuan, Ionic liquids for high performance lithium metal batteries, *J. Energy Chem.*, 59(2021), p. 320.
[52] D.J. Yoo, K.J. Kim, and J.W. Choi, The synergistic effect of cation and anion of an ionic liquid additive for lithium metal anodes, *Adv. Energy Mater.*, 8(2018), No. 11, art. No. 1702744.